STRUCTURAL BIOLOGY COMMUNICATIONS

ISSN 2053-230X

Crystal structure of RecR, a member of the RecFOR DNA-repair pathway, from *Pseudomonas aeruginosa* PAO1

Shiyou Che,[a] Yujing Chen,[a] Yakun Liang,[a] Qionglin Zhang[a]* and Mark Bartlam[a,b]*

[a]College of Life Sciences, Nankai University, 94 Weijin Road, Tianjin 300071, People's Republic of China, and [b]State Key Laboratory of Medicinal Chemical Biology, Nankai University, 38 Tongyan Road, Tianjin 300350, People's Republic of China. *Correspondence e-mail: zql@nankai.edu.cn, bartlam@nankai.edu.cn

Received 9 January 2018
Accepted 28 February 2018

Edited by S. Sheriff, Bristol-Myers Squibb, USA

Keywords: crystal structure; homologous recombination; RecR; DNA repair; *Pseudomonas aeruginosa*.

PDB reference: RecR, 5z2v

Supporting information: this article has supporting information at journals.iucr.org/f

DNA damage is usually lethal to all organisms. Homologous recombination plays an important role in the DNA damage-repair process in prokaryotic organisms. Two pathways are responsible for homologous recombination in *Pseudomonas aeruginosa*: the RecBCD pathway and the RecFOR pathway. RecR is an important regulator in the RecFOR homologous recombination pathway in *P. aeruginosa*. It forms complexes with RecF and RecO that can facilitate the loading of RecA onto ssDNA in the RecFOR pathway. Here, the crystal structure of RecR from *P. aeruginosa* PAO1 (*Pa*RecR) is reported. *Pa*RecR crystallizes in space group $P6_122$, with two monomers per asymmetric unit. Analytical ultracentrifugation data show that *Pa*RecR forms a stable dimer, but can exist as a tetramer in solution. The crystal structure shows that dimeric *Pa*RecR forms a ring-like tetramer architecture *via* crystal symmetry. The presence of a ligand in the Walker B motif of one RecR subunit suggests a putative nucleotide-binding site.

1. Introduction

Maintaining genomic integrity and stability is crucial for all organisms. Damage to DNA is unavoidable following exposure to ultraviolet radiation, ionizing radiation and chemical mutagens (Inoue *et al.*, 2008; Lindahl, 1993). Cells have therefore evolved several different mechanisms to maintain the structural and informational fidelity of their DNA, including homologous recombination, nonhomologous end joining, base-excision repair, nucleotide-excision repair, mismatch repair and reversion repair (West, 2003; Burma *et al.*, 2006; Shuman & Glickman, 2007). In all cells, homologous recombination plays a key role in the generation of genetic diversity, the maintenance of genomic integrity and the proper segregation of chromosomes (Cox *et al.*, 2000; Spies & Kowalczykowski, 2005). In wild-type *Escherichia coli*, two distinct recombination pathways are responsible for the repair of DNA damage by recombination: the RecBCD pathway and the RecFOR (or RecF) pathway (Kowalczykowski *et al.*, 1994; Tseng *et al.*, 1994; Kowalczykowski, 2000). These pathways are conserved in the opportunistic pathogen *Pseudomonas aeruginosa* PAO1. The *recF* gene in *P. aeruginosa* PAO1 has been shown to be downregulated following treatment with the antibiotic ciprofloxacin as part of the SOS response system (Cirz *et al.*, 2006).

In prokaryotic cells, RecA is important for strand exchange during homologous recombination, stabilizing stalled replication forks. The RecBCD and RecF pathways both load RecA onto single-stranded DNA (ssDNA) to allow homologous strand invasion, but differ in the type of damaged DNA that

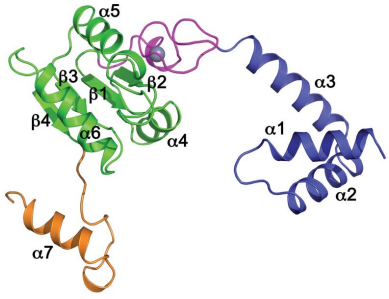

© 2018 International Union of Crystallography

they can repair (Bork *et al.*, 2001; Cox, 2007; Lenhart *et al.*, 2014). RecBCD is a multifunctional enzyme complex with highly processive helicase activity, ATP-dependent exonuclease activity and RecA-loading activity (Singleton *et al.*, 2004; Dillingham & Kowalczykowski, 2008). The RecBCD pathway is responsible for the repair initiated at double-stranded DNA (dsDNA) breaks. During the repair process, RecBCD generates a 3′ ssDNA extension after encountering a Chi site and facilitates the loading of RecA onto ssDNA produced by its helicase/nuclease activity (Spies & Kowalczykowski, 2006; Spies *et al.*, 2007; Dillingham & Kowalczykowski, 2008).

Compared with the RecBCD pathway, the RecF pathway is mainly responsible for single-stranded DNA damage, and requires several proteins (RecA, RecF, RecO, RecR, RecJ and RecQ) to process the DNA into a presynaptic intermediate. The DNA is unwound by the RecQ helicase and the 5′ end is digested by RecJ, leaving the 30-tailed ssDNA coated with single-stranded DNA-binding proteins (SSBs). RecR and RecO form a complex that directs the specific loading of the RecA protein onto ssDNA; RecF can accelerate this process and ATP is needed at the same time (Umezu & Kolodner, 1994; Ryzhikov *et al.*, 2011; Morimatsu *et al.*, 2012).

To date, crystal structures of RecR have been determined from *Thermoanaerobacter tengcongensis* (also known as *Caldanaerobacter subterraneus*) and *Deinococcus radiodurans*, revealing that RecR forms a DNA clamp-like tetramer architecture that encircles dsDNA by forming a complex with RecO and RecF (Honda *et al.*, 2008; Tang *et al.*, 2012; Radzimanowski *et al.*, 2013; Lee *et al.*, 2004). In order to elucidate the structure of RecR from *P. aeruginosa* PAO1 (*Pa*RecR), the *recR* (*pa1534*) gene was cloned for overexpression in *E. coli*, and *Pa*RecR was purified and crystallized. Here, we report the crystal structure of *Pa*RecR determined to 2.2 Å resolution.

2. Materials and methods

2.1. Macromolecule production

The *recR* (*pa1534*) gene was amplified by polymerase chain reaction using the genome of *P. aeruginosa* PAO1 as a template, and the PCR product of full-length PA1534 (residues 1–197) was cloned into the pGEX-6p-1 vector (GE Healthcare, Beijing, People's Republic of China). For expression of RecR, the recombinant plasmid for RecR was transformed into *E. coli* strain BL21(DE3) and the cells were grown in 1 l Luria–Bertani broth medium containing 100 µg ml^{-1} ampicillin at 310 K. When the OD_{600} reached 0.5, isopropyl β-D-1-thiogalactopyranoside (IPTG) was added to the growth medium to a final concentration of 0.5 m*M* to induce the expression of recombinant protein. The induced cultures were grown at 289 K for 18 h. The cells were harvested by centrifugation at 4000*g* for 15 min, resuspended in 25 ml lysis buffer (25 m*M* Tris, 50 m*M* NaCl pH 8.5) and then lysed using a high-pressure homogenizer (ATS Nano Technology, Suzhou, People's Republic of China) at 277 K. Cell debris was removed by centrifugation at 40 000*g* for 40 min at 277 K. The supernatant was loaded onto a GST column (GE Healthcare) equilibrated with lysis buffer. The column was washed five times with 100 ml lysis buffer. Finally, 0.6 mg PreScission Protease (GE Healthcare) was added to the resin to remove the GST tag. The protein was eluted with 25 m*M* Tris, 20 m*M* NaCl pH 8.0 and then concentrated and purified using anion-exchange chromatography on a HiTrap Q column (GE Healthcare). The protein was further purified using a Superdex 200 Increase 10/300 GL column (GE Healthcare) equilibrated with 20 m*M* Tris, 100 m*M* NaCl pH 8.0. The purified protein was concentrated to 10 mg ml^{-1} using an Amicon Ultra centrifugal filter unit (Millipore; molecular-weight cutoff 30 kDa) and stored at 193 K. Macromolecule-production information is summarized in Table 1.

Table 1
Macromolecule production.

The BamHI site and the EcoRI site are underlined. The tag residues removed by PreScission protease are shown in italics.

Source organism	*P. aeruginosa* PAO1
DNA source	Genome
Forward primer	CGCGGATCCATGAGTTTCAGCCCGCTGATCC
Reverse primer	CCGGAATTCTCAGGAGATCGGCCGCCGTCCG
Cloning vector	pGEX-6P-1
Expression vector	pGEX-6p-1
Expression host	*E. coli* BL21(DE3)
Complete amino-acid sequence of the construct produced	*GPLGS*MSFSPLIRQLIESLRILPGVGQKSAQ RMALMLLERDRSGGLKLAQALTAAMEGVG HCRQCRTLSEEELCPQCADPRRDDSLLCV VEGPLDVFAVEQTGYRGRYFVLKGHLSPL DGLGPEAIGIPELEARIRDGAFSEVILAT NPTVEGEATAHYIAQLLAGRGLTLSRIAH GVPLGGELELVDGGTLAHALAGRRPIS

2.2. Analytical ultracentrifugation

Analytical ultracentrifugation (AUC) was performed in sedimentation-velocity mode using a Beckman Coulter XL-I analytical ultracentrifuge (Beckman Instruments, Palo Alto, California, USA) with two-channel centrepieces and sapphire windows at 277 K and a rotor speed of 42 000 rev min^{-1} (142 000*g*) with interference detection. The purified protein was diluted to 1 mg ml^{-1} in 20 m*M* Tris, 100 m*M* NaCl pH 8.0 buffer. The protein partial specific volume and buffer density were estimated using *SEDNTERP*, and the sedimentation-equilibration data were analysed by the $c(s)$ or ls-$g^*(s)$ method using the *SEDFIT* software (Dam & Schuck, 2004).

2.3. Crystallization

Crystallization screening for RecR was carried out using the sitting-drop vapour-diffusion method with the commercial kits Crystal Screen, Crystal Screen 2 and Index (Hampton Research, Aliso Viejo, California, USA) in 48-well sitting-drop plates. Snowflake-shaped crystals were observed after 3 d using Index condition No. 17 consisting of 1.26 *M* sodium phosphate monobasic monohydrate, 0.14 *M* potassium phosphate dibasic. For crystal optimization, reservoir solutions were prepared by mixing 80 µl Index condition No. 17 and 20 µl of each of the solutions from the commercial

Table 2
Crystallization.

Method	Sitting-drop vapour diffusion
Plate type	48-well
Temperature (K)	289
Protein concentration (mg ml^{-1})	5
Buffer composition of protein solution	25 m*M* Tris–HCl, 100 m*M* NaCl pH 8.5
Composition of reservoir solution	80 µl 1.26 *M* sodium phosphate monobasic monohydrate, 0.14 *M* potassium phosphate dibasic and 20 µl 10%(*w*/*v*) PEG 6000, 100 m*M* HEPES–NaOH pH 7.0
Volume and ratio of drop	2 µl; 1:1 ratio of protein:reservoir
Volume of reservoir	100 µl

Table 3
Data collection and processing.

Values in parentheses are for the outer shell.

Diffraction source	BL19U1, SSRF
Wavelength (Å)	0.97776
Temperature (K)	100
Detector	PILATUS3 6M
Crystal-to-detector distance (mm)	400.00
Rotation range per image (°)	0.5
Total rotation range (°)	360
Exposure time per image (s)	0.5
Space group	$P6_122$
a, *b*, *c* (Å)	70.1, 70.1, 369.0
α, β, γ (°)	90, 90, 120
Mosaicity (°)	0.3
Resolution range (Å)	50.00–2.20 (2.24–2.20)
Total No. of reflections	621073
No. of unique reflections	27394 (2318)
Completeness (%)	99.7 (97.9)
Multiplicity	21.4 (16.0)
$\langle I/\sigma(I)\rangle$	20.3 (3.3)
$CC_{1/2}$	0.999 (0.949)
$R_{r.i.m.}$	0.034 (0.215)
Overall *B* factor from Wilson plot (Å^2)	35

Wizard 1 & 2 screening kits (Rigaku Reagents). This optimization strategy was based on the protocol described by Birtley & Curry (2005), whereby commercial screening solutions are employed as additives once initial crystallization conditions have been obtained. The optimized crystals were finally obtained with reservoir solution consisting of 80 µl 1.26 *M* sodium phosphate monobasic monohydrate, 0.14 *M* potassium phosphate dibasic and 20 µl Wizard 1 condition No. 20 [10%(*w*/*v*) PEG 6000, 100 m*M* HEPES–NaOH pH 7.0]. Crystallization information is summarized in Table 2.

2.4. Data collection and processing

Prior to data collection, crystals were cryoprotected by adding 20%(*v*/*v*) glycerol to the crystallization buffer before flash-cooling them in liquid nitrogen. The *Pa*RecR diffraction data set was collected on beamline BL19U1 of the Shanghai Synchrotron Radiation Facility (SSRF) at 100 K. Data sets were integrated, scaled and merged using the *HKL*-2000 suite (Otwinowski & Minor, 1997). Data-collection and processing statistics are summarized in Table 3.

Table 4
Structure solution and refinement.

Values in parentheses are for the outer shell.

Resolution range (Å)	36.72–2.19 (2.25–2.19)
Completeness (%)	94.5 (80.9)
No. of reflections, working set	27392 (2317)
No. of reflections, test set	1895 (165)
Final R_{cryst}†	0.189 (0.245)
Final R_{free}†	0.221 (0.254)
No. of non-H atoms	
Protein	2938
Ions (Na^+, Zn^{2+}, PO_4^{3-})	8
Ligand	25
Water	182
Total	3153
R.m.s. deviations	
Bonds (Å)	0.016
Angles (°)	1.8
Average *B* factors (Å^2)	
Protein	30
Ions (Na^+, Zn^{2+}, PO_4^{3-})	36
Ligand	58
Water	35
Ramachandran plot‡	
Most favoured (%)	97.9
Allowed (%)	2.1

† $R_{cryst} = \sum_{hkl} ||F_{obs}| - |F_{calc}|| / \sum_{hkl} |F_{obs}|$; R_{free} is the *R* factor for a selected subset of the reflections that was not included in refinement calculations. ‡ Ramachandran plot calculated using *MolProbity* (Chen *et al.*, 2010).

2.5. Structure solution and refinement

The structure of *Pa*RecR was determined by molecular replacement with *Phaser* (McCoy *et al.*, 2007) in the *PHENIX* suite (Adams *et al.*, 2010) using a monomer of *T. tengcongensis* RecR (PDB entry 3vdp; 48% sequence identity; Tang *et al.*, 2012) as a search model. The molecular-replacement model was subjected to automatic building using *AutoBuild* in *PHENIX*, which built 386 residues in two chains. The structure of *Pa*RecR was then refined with *PHENIX* (Adams *et al.*, 2010) combined with cycles of manual building in *Coot* (Emsley *et al.*, 2010). The final model was optimized using *PDB_REDO* (Joosten *et al.*, 2014). The structure was validated with *MolProbity* (Chen *et al.*, 2010). All structure figures were drawn with *PyMOL* (v.2.0; Schrödinger). Refinement statistics are summarized in Table 4.

3. Results and discussion

3.1. The structure of *P. aeruginosa* RecR

The full-length purified recombinant RecR protein (Figs. 1*a* and 1*b*) from *P. aeruginosa* PAO1 (*Pa*RecR; residues 1–197) was crystallized with symmetry consistent with space group $P6_122$ with two monomers in an asymmetric unit, corresponding to a Matthews coefficient of 2.94 Å^3 Da^{-1} and an estimated solvent content of 58%. Analytical ultracentrifugation analysis confirms that *Pa*RecR largely forms a homodimer in solution, as shown by a peak at ∼46 kDa corresponding to twice the theoretical monomer molecular mass of 21 kDa (Fig. 1*c*). A secondary peak at ∼107 kDa also indicates the presence of homotetramers in solution. The resulting structure was refined to 2.2 Å resolution and includes

two *Pa*RecR monomers in an asymmetric unit, forming a stable dimer involving exchange of the N-terminal domains. The quality of the experimental electron-density maps was good (Supplementary Fig. S1), such that subunit *A* could be traced in continuous electron density from residues 3 to 197 and subunit *B* from residues 1 to 197. The two RecR monomers in an asymmetric unit adopt a similar conformation, with an r.m.s.d. of 1.1 Å for 195 C^{α} atoms.

The structure of the *Pa*RecR monomer, which has approximate dimensions of 70 × 50 × 40 Å, is divided into three regions (Fig. 1*d*). The N-terminal region is composed of a helix–hairpin–helix (HhH) motif (residues 1–54). The HhH

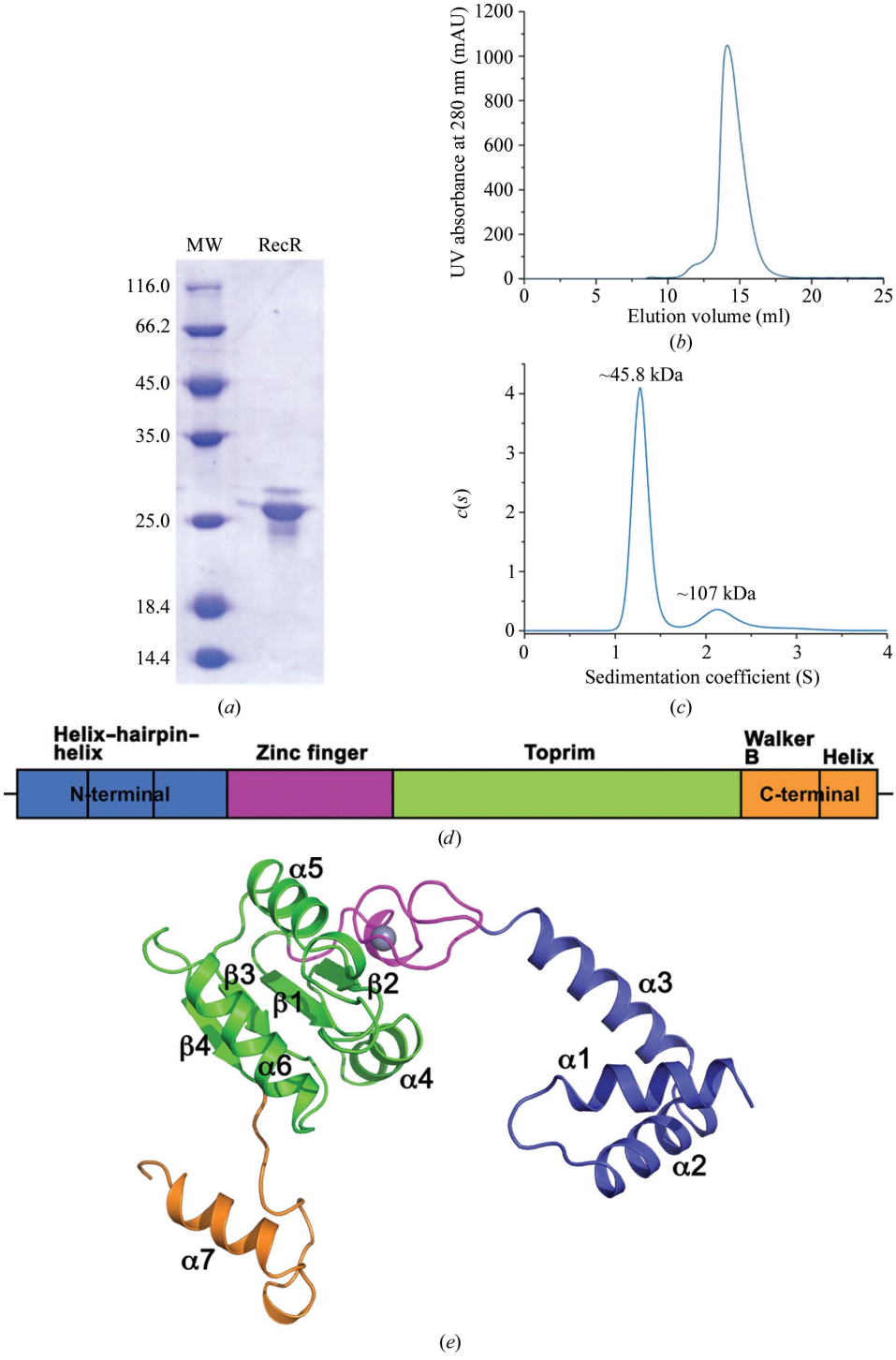

Figure 1
The *Pa*RecR structure. (*a*) A representative SDS–PAGE gel (stained with Coomassie Blue) of the main peak eluted from the size-exclusion chromatography column, with molecular-weight markers shown (lane MW; labelled in kDa). (*b*) Elution profile of full-length *Pa*RecR (residues 1–197) from a Superdex 200 10/300 GL size-exclusion chromatography column with absorbance measured at 280 nm. (*c*) Analytical ultracentrifugation profile of *Pa*RecR. (*d*) The *Pa*RecR monomer structure coloured according to the domain orientation shown above: blue, N-terminal helix–hairpin–helix motif; magenta, Cys_4 zinc-finger motif; green, Toprim domain; orange, C-terminal Walker B motif.

motif is formed by helices $\alpha1$ and $\alpha2$, with an additional helix $\alpha3$ linking the HhH motif to the Cys_4 zinc-finger motif. The HhH motif is associated with DNA binding, and in the context of RecR has been shown to be essential for DNA binding and association with RecO (Lee *et al.*, 2004).

The middle region consists of a zinc-finger motif (residues 55–78) and a Toprim domain (residues 79–167). The Cys_4 zinc-finger motif consists of four strictly conserved cysteine residues (Cys69, Cys72, Cys57 and Cys60) which coordinate a zinc ion. The Cys_4 zinc finger lies on the outside of the RecR monomer. An *E. coli* strain carrying RecR with a mutated zinc finger showed reduced survival (Clark, 1991), suggesting its importance for the function of RecR, most likely in DNA binding. The Toprim domain resembles a Rossmann-like nucleotide-binding fold with a parallel four-stranded β-sheet flanked on one side by one α-helix ($\alpha4$) and on the other by two α-helices ($\alpha5$ and $\alpha6$). The Toprim domain in RecR lacks the fingerprint acidic D*x*D sequence found in the Toprim domains of topoisomerases, but is rich in conserved acidic residues.

The C-terminal region (residues 168–197) includes a Walker B motif and a C-terminal helix. The Walker B motif in RecR has a sequence motif that diverges from the signature motif (R/K)*xxx*G*xxx*(L/V)*hhhh*DE, where *x* is any residue and *h* is a hydrophobic residue (Hanson & Whiteheart, 2005). The aspartate in the consensus Walker B motif coordinates the magnesium required for ATP hydrolysis, and the glutamate is thought to prime a water molecule for nucleophilic attack (Hanson & Whiteheart, 2005). In *Pa*RecR, the Walker B motif, with sequence $_{168}$RIAHGVPLGGELELVDG$_{184}$, forms a long loop with a 3_{10}-helix at its C-terminus and is followed by the C-terminal helix $\alpha7$. *Pa*RecR lacks the catalytic glutamate of the consensus Walker B motif; mutation at this position has been linked to impaired ATP hydrolysis but not ATP binding (Hanson & Whiteheart, 2005).

A *DALI* search for structural homology reveals closest similarity to the published monomeric structures of the RecR proteins from *T. tengcongensis* (PDB entry 3vdp; *Z*-score 22, r.m.s.d. of 1.7 Å for 195 aligned residues; 48% sequence identity; Tang *et al.*, 2012) and *D. radiodurans* (PDB entry 2v1c; *Z*-score 20.4; r.m.s.d. of 1.9 Å for 193 aligned residues; 48% sequence identity; Timmins *et al.*, 2007). The *P. aeruginosa*, *T. tengcongensis* and *D. radiodurans* RecR structures all share a similar fold but exhibit slightly different domain orientations (Fig. 2).

3.2. The *P. aeruginosa* RecR dimer and tetramer structures

RecR proteins are reported to have different oligomeric states in solution. *D. radiodurans* and *Helicobacter pylori* RecR have been shown to be tetrameric in solution at a concentration of 1 mg ml^{-1} by analytical ultracentrifugation (Lee *et al.*, 2004), but more recently *D. radiodurans* RecR was shown to be dimeric in solution by SAXS analysis (Radzimanowski *et al.*, 2013). Analytical ultracentrifugation confirms that *P. aeruginosa* RecR is predominantly dimeric at a concentration of 1 mg ml^{-1}, but also exists as a tetramer at the same concentration. This ability to transition between dimers and tetramers has been ascribed to the ability of RecR tetramers to open and close at intracellular concentrations (Lee *et al.*, 2004), thus enabling it to act as a clamp protein to encircle DNA.

Two RecR monomers in the asymmetric unit form a dimer (termed the N–N dimer) with domain-swapped N-terminal helix–hairpin–helix (HhH) motifs (Fig. 3*a*). This dimer has a buried interface area of ∼2400 Å^2 and a solvation free-energy gain ΔG of −48.4 kcal mol^{-1} as calculated using *PISA* (Krissinel & Henrick, 2007). This region has been shown to be essential for the interaction with RecO in *T. tengcongensis* (Tang *et al.*, 2012). Deletion of the N-terminal 15 amino acids from *T. tengcongensis* RecR also results in the formation of a dimer, but one which is unable to form a complex with RecO in solution (Tang *et al.*, 2012).

A ring-like tetramer is generated from the N–N dimer *via* a twofold-symmetry transformation (Fig. 3*b*) and is consistent with the ring-like structures observed for the *T. tengcongensis* and *D. radiodurans* RecR structures (Lee *et al.*, 2004; Tang *et al.*, 2012). The *Pa*RecR tetramer can be superimposed onto the *T. tengcongensis* RecR tetramer with an r.m.s.d. of 2.7 Å for 701 aligned residues, showing good overall agreement between the two tetramers. The N-terminal HhH and C-terminal Walker B motifs involved in dimerization align closely, but the Toprim domains of the two structures align less closely. In particular, a large deviation of as much as 12 Å is observed between loop 106–121 of the *Pa*RecR (chain *B*) and *T. tengcongensis* RecR (chains *B* and *D*) structures. This loop has been reported to bind tightly into a hydrophobic pocket in RecO and is crucial for the interaction of RecR with RecO (Tang *et al.*, 2012).

The dimensions of the tetramer are roughly 90 × 70 × 30 Å, with a central hole of approximately 35 × 30 Å. The tetramer is formed by interactions between subunits *A*–*A*′ and subunits *B*–*B*′, with a buried interface area of ∼2000 Å^2 and a solvation free-energy gain ΔG of −32.1 kcal mol^{-1} for each pair of subunits. This generates another dimer interface (termed the C–C dimer) in which the C-terminal Walker B motifs are domain-swapped (Fig. 3*b*). *Pa*RecR lacks the C-terminal

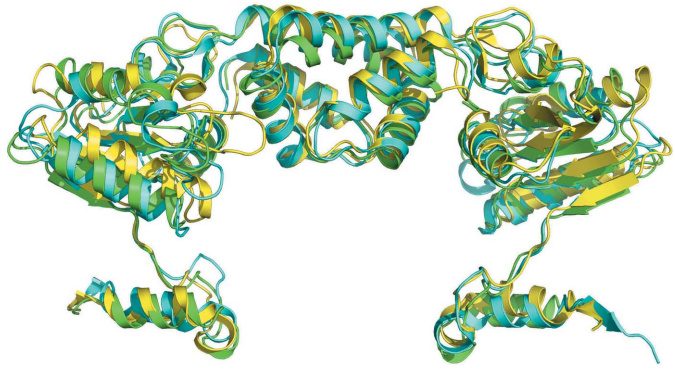

Figure 2
Superposition of *Pa*RecR (green), *D. radiodurans* RecR (cyan; PDB entry 1vdd; Lee *et al.*, 2004) and *T. tengcongensis* RecR (yellow; PDB entry 3vdp; Tang *et al.*, 2012) homodimer structures. All structures are shown in cartoon representation.

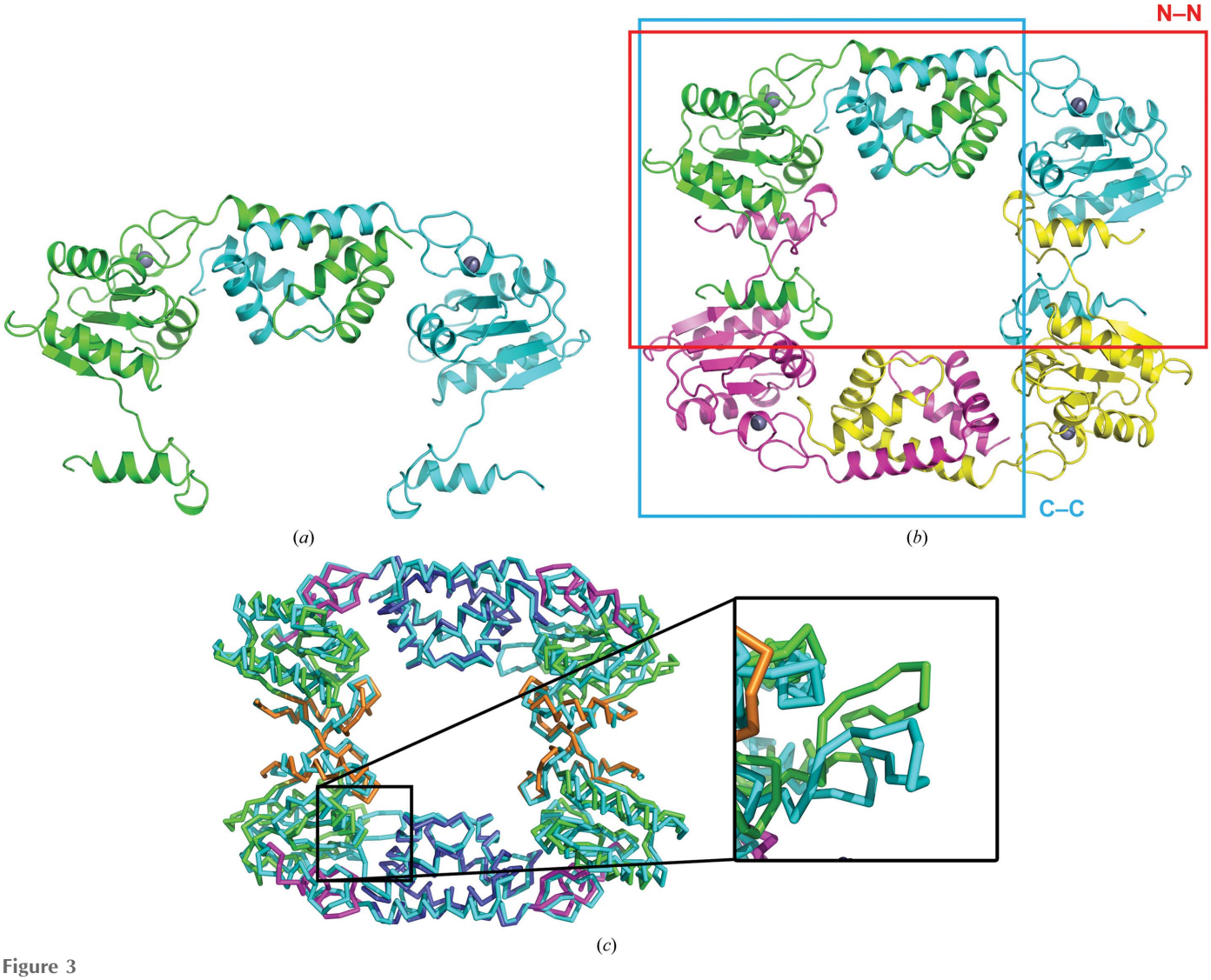

Figure 3
The *Pa*RecR dimer and tetramer structures. (*a*) The *Pa*RecR N–N dimer structure, shown in ribbon representation. Subunit *A* is coloured green and subunit *B* is coloured cyan. (*b*) The *Pa*RecR tetramer structure shown in ribbon representation. Subunit *A* is coloured green, subunit *B* is coloured cyan, subunit *A*′ is coloured magenta and subunit *B*′ is coloured yellow. The N–N and C–C dimers are shown by red and blue boxes, respectively. (*c*) Superposition of *Pa*RecR and *T. tengcongensis* RecR tetramers. Both tetramers are shown in *PyMOL* ribbon representation; *Pa*RecR is coloured according to structural domain (blue, HhH motif; magenta, zinc-finger motif; green, Toprim domain; orange, Walker B motif) and *T. tengcongensis* RecR is coloured cyan. Inset: comparison of loop 106–121 of the two structures.

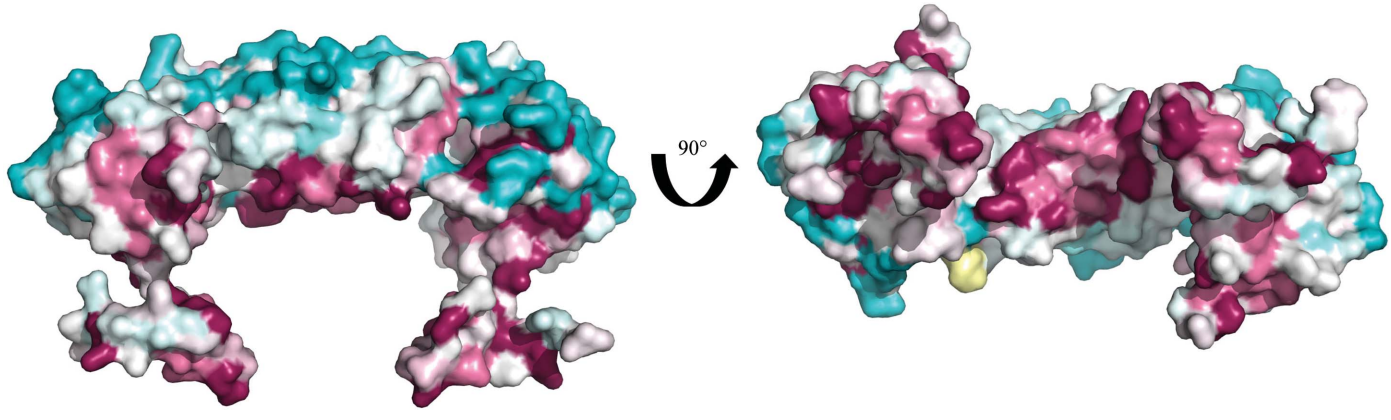

Figure 4
ConSurf analysis of the *Pa*RecR dimer. The *Pa*RecR dimer is shown in surface representation and coloured according to conservation calculated from 150 homologous sequences, from turquoise (low conservation) through white (average conservation) to maroon (high conservation).

β-strand β7 observed in the *D. radiodurans* RecR structure, which lies antiparallel to the central β-sheet of the Toprim domain from a neighbouring monomer (Lee *et al.*, 2004), but the mode of C–C dimerization is otherwise identical.

A *ConSurf* analysis (Ashkenazy *et al.*, 2016) of the *Pa*RecR structure with 150 unique homologous sequences revealed that the most conserved regions are on the inner surface of the protein lining the central hole, including the N-terminal HhH motif and the C-terminal Walker B motif (Fig. 4). This suggests a high conservation of function, as both the HhH motif and the Walker B motif are implicated in binding to DNA and to RecO.

3.3. A ligand-binding site in the RecR Walker B motif

Careful examination of the electron-density maps identified a region of electron density in chain *A* corresponding to an unidentified ligand sandwiched between helix α6 in the Toprim domain and helix α7 in the Walker B motif (Fig. 5*a*). The Walker B motif is associated with ATP binding and ATP hydrolysis. In the context of RecR, an increase in α-helical content in *D. radiodurans* and *H. pylori* RecR was observed by circular-dichroism spectroscopy in the presence of ATP, suggesting that the Walker B motif undergoes a conformational change upon ATP binding (Lee *et al.*, 2004). No ATPase activity was detected for *D. radiodurans*, *H. pylori* or *Streptomyces coelicolor* RecR (Lee *et al.*, 2004; Peláez *et al.*, 2001), although the DNA-binding activity of *Bacillus subtilis* RecR was observed to be increased by ATP (Alonso *et al.*, 1993). The size and shape of the electron density for the unidentified ligand is consistent with the ribose and phosphate moieties of a nucleotide, as shown by a $2mF_o - DF_c$ OMIT map (Fig. 5*a*) and a polder OMIT map (Fig. 5*b*; Liebschner *et*

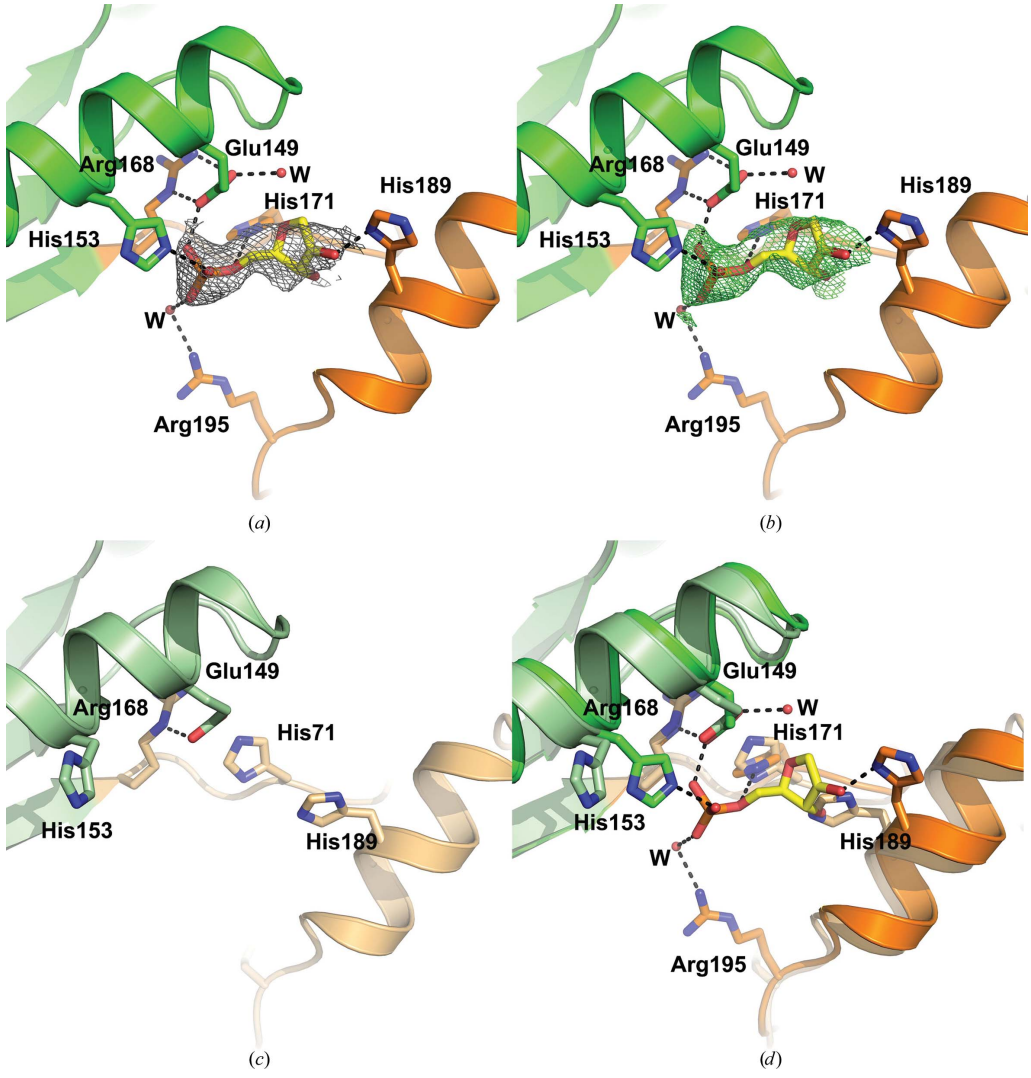

Figure 5
Ligand binding in the Walker B motif. (*a*) The ligand-binding site in subunit *A* of *Pa*RecR. The ligand is shown in yellow stick representation and is covered by a $2mF_o - DF_c$ OMIT electron-density map shown as a grey mesh and contoured at 1.6 r.m.s.d. Residues coordinating the ligand are shown in stick representation and are coloured according to the scheme in Fig. 1(*c*) (blue, HhH motif; magenta, zinc-finger motif; green, Toprim domain; orange, Walker B motif). (*b*) The ligand in subunit *A* of *Pa*RecR covered by a polder OMIT electron-density map shown as a green mesh and contoured at 3.0 r.m.s.d. (*c*) The equivalent ligand-free site in subunit *B* of *Pa*RecR. Residues are shown in stick representation and are coloured pale green for the Toprim domain and pale orange for the Walker B motif. (*d*) Superposition of the ligand-binding sites in subunits *A* (Toprim domain in green, Walker B motif in orange) and *B* (Toprim domain in pale green, Walker B motif in pale orange).

al., 2017). The phosphate group is coordinated by Glu149, which forms a salt bridge to Arg168, His153 in the Toprim domain, and His171 and Arg195 (*via* a water molecule) in the Walker B motif. The ribose moiety is coordinated by His189 in the Walker B motif.

The ligand binding is asymmetrical, as no corresponding electron density is observed in chain *B* (Fig. 5*c*). The side chain of His171 in chain *B* instead interacts with the side chain of Glu141. The side chain of His189 in chain *B* rotates to occupy the position of the ribose moiety, and the side chains of His153 and Arg195 are directed out of the putative ligand-binding pocket. Superposition of chains *A* and *B* shows a movement of the Walker B motif by approximately 2 Å and of helix α7 by approximately 2.5 Å away from the Toprim domain in subunit *A*, indicating a minor conformational change to accommodate the ligand (Fig. 5*d*).

The ligand-binding site in subunit *A* of *Pa*RecR is distinct from the typical ATP-binding site observed in the Walker B motifs of proteins such as the AAA+ (ATPases associated with various cellular activities) family. The Walker B motif in AAA+ proteins forms contacts with the nucleotide: the aspartate residue in the *hhhh*DE sequence coordinates the magnesium required for ATP hydrolysis, and the glutamate activates water for the hydrolysis reaction (Hanson & Whiteheart, 2005). Asp183 in the *hhhh*DE sequence of *Pa*RecR is situated approximately 10 Å from the ribose moiety of the ligand, while the glutamate in the *hhhh*DE sequence is substituted by Gly184. Mutation of the catalytic glutamate in the *hhhh*DE sequence is reported to abolish ATP hydrolysis but not ATP binding (Hanson & Whiteheart, 2005), suggesting that *Pa*RecR might lack ATP-hydrolysis activity, consistent with other RecR proteins (Lee *et al.*, 2004; Peláez *et al.*, 2001). Further work is under way to investigate the relevance of this ligand-binding site as a putative ATP- or nucleotide-binding site, and to investigate the effects of ATP on the DNA-binding activity.

4. Conclusions

In summary, we have determined the 2.2 Å resolution structure of RecR, a member of the RecF homologous recombination pathway, from *P. aeruginosa* PAO1. *Pa*RecR is predominantly a dimer in solution but can exist as a tetramer. The crystal structure confirms the existence of a *Pa*RecR tetramer, consistent with other members of the RecR family. A ligand identified in the Walker B motif, which is associated with ATP binding and hydrolysis, suggests a putative nucleotide-binding site. Further work is under way to examine the function of RecR and to characterize its interaction with ssDNA or with its known binding partners, RecO or RecF.

Acknowledgements

We thank the staff of the National Center for Protein Sciences Shanghai (NCPSS) beamline BL19U at Shanghai Synchrotron Radiation Facility for assistance during data collection.

Funding information

The following funding is acknowledged: National Natural Science Foundation of China (grant No. 31570128); Tianjin Municipal Science and Technology Commission (grant No. 13JCYBJC20800).

References

Adams, P. D. *et al.* (2010). *Acta Cryst.* D**66**, 213–221.
Alonso, J. C., Stiege, A. C., Dobrinski, B. & Lurz, R. (1993). *J. Biol. Chem.* **268**, 1424–1429.
Ashkenazy, H., Abadi, S., Martz, E., Chay, O., Mayrose, I., Pupko, T. & Ben-Tal, N. (2016). *Nucleic Acids Res.* **44**, W344–W350.
Birtley, J. R. & Curry, S. (2005). *Acta Cryst.* D**61**, 646–650.
Bork, J. M., Cox, M. M. & Inman, R. B. (2001). *EMBO J.* **20**, 7313–7322.
Burma, S., Chen, B. P. C. & Chen, D. J. (2006). *DNA Repair*, **5**, 1042–1048.
Chen, V. B., Arendall, W. B., Headd, J. J., Keedy, D. A., Immormino, R. M., Kapral, G. J., Murray, L. W., Richardson, J. S. & Richardson, D. C. (2010). *Acta Cryst.* D**66**, 12–21.
Cirz, R. T., O'Neill, B. M., Hammond, J. A., Head, S. R. & Romesberg, F. E. (2006). *J. Bacteriol.* **188**, 7101–7110.
Clark, A. J. (1991). *Biochimie*, **73**, 523–532.
Cox, M. M. (2007). *Crit. Rev. Biochem. Mol. Biol.* **42**, 41–63.
Cox, M. M., Goodman, M. F., Kreuzer, K. N., Sherratt, D. J., Sandler, S. J. & Marians, K. J. (2000). *Nature (London)*, **404**, 37–41.
Dam, J. & Schuck, P. (2004). *Methods Enzymol.* **384**, 185–212.
Dillingham, M. S. & Kowalczykowski, S. C. (2008). *Microbiol. Mol. Biol. Rev.* **72**, 642–671.
Emsley, P., Lohkamp, B., Scott, W. G. & Cowtan, K. (2010). *Acta Cryst.* D**66**, 486–501.
Hanson, P. I. & Whiteheart, S. W. (2005). *Nature Rev. Mol. Cell Biol.* **6**, 519–529.
Honda, M., Fujisawa, T., Shibata, T. & Mikawa, T. (2008). *Nucleic Acids Res.* **36**, 5013–5020.
Inoue, J., Honda, M., Ikawa, S., Shibata, T. & Mikawa, T. (2008). *Nucleic Acids Res.* **36**, 94–109.
Joosten, R. P., Long, F., Murshudov, G. N. & Perrakis, A. (2014). *IUCrJ*, **1**, 213–220.
Kowalczykowski, S. C. (2000). *Trends Biochem. Sci.* **25**, 156–165.
Kowalczykowski, S. C., Dixon, D. A., Eggleston, A. K., Lauder, S. D. & Rehrauer, W. M. (1994). *Microbiol. Rev.* **58**, 401–465.
Krissinel, E. & Henrick, K. (2007). *J. Mol. Biol.* **372**, 774–797.
Lee, B. I., Kim, K. H., Park, S. J., Eom, S. H., Song, H. K. & Suh, S. W. (2004). *EMBO J.* **23**, 2029–2038.
Lenhart, J. S., Brandes, E. R., Schroeder, J. W., Sorenson, R. J., Showalter, H. D. & Simmons, L. A. (2014). *J. Bacteriol.* **196**, 2851–2860.
Liebschner, D., Afonine, P. V., Moriarty, N. W., Poon, B. K., Sobolev, O. V., Terwilliger, T. C. & Adams, P. D. (2017). *Acta Cryst.* D**73**, 148–157.
Lindahl, T. (1993). *Nature (London)*, **362**, 709–715.
McCoy, A. J., Grosse-Kunstleve, R. W., Adams, P. D., Winn, M. D., Storoni, L. C. & Read, R. J. (2007). *J. Appl. Cryst.* **40**, 658–674.
Morimatsu, K., Wu, Y. & Kowalczykowski, S. C. (2012). *J. Biol. Chem.* **287**, 35621–35630.
Otwinowski, Z. & Minor, W. (1997). *Methods Enzymol.* **276**, 307–326.
Peláez, A. I., Ribas-Aparicio, R. M., Gómez, A. & Rodicio, M. R. (2001). *Mol. Genet. Genomics*, **265**, 663–672.
Radzimanowski, J., Dehez, F., Round, A., Bidon-Chanal, A., McSweeney, S. & Timmins, J. (2013). *Nucleic Acids Res.* **41**, 7972–7986.
Ryzhikov, M., Koroleva, O., Postnov, D., Tran, A. & Korolev, S. (2011). *Nucleic Acids Res.* **39**, 6305–6314.
Shuman, S. & Glickman, M. S. (2007). *Nature Rev. Microbiol.* **5**, 852–861.

Singleton, M. R., Dillingham, M. S., Gaudier, M., Kowalczykowski, S. C. & Wigley, D. B. (2004). *Nature (London)*, **432**, 187–193.
Spies, M., Amitani, I., Baskin, R. J. & Kowalczykowski, S. C. (2007). *Cell*, **131**, 694–705.
Spies, M. & Kowalczykowski, S. C. (2005). *The Bacterial Chromosome*, edited by N. P. Higgins, pp. 389–403. Washington DC: ASM Press.
Spies, M. & Kowalczykowski, S. C. (2006). *Mol. Cell*, **21**, 573–580.
Tang, Q., Gao, P., Liu, Y.-P., Gao, A., An, X.-M., Liu, S., Yan, X.-X. & Liang, D.-C. (2012). *Nucleic Acids Res.* **40**, 11115–11125.
Timmins, J., Leiros, I. & McSweeney, S. (2007). *EMBO J.* **26**, 3260–3271.
Tseng, Y.-C., Hung, J.-L. & Wang, T.-C. V. (1994). *Mutat. Res.* **315**, 1–9.
Umezu, K. & Kolodner, R. D. (1994). *J. Biol. Chem.* **269**, 30005–30013.
West, S. C. (2003). *Nature Rev. Mol. Cell Biol.* **4**, 435–445.